Molecular Communication using Magnetic Nanoparticles

Wayan Wicke
Arman Ahmadzadeh
Vahid Jamali
Robert Schober
Friedrich-Alexander Universität Erlangen-Nürnberg
Institute for Digital Communications

Harald Unterweger
Christoph Alexiou
Universitätsklinikum Erlangen
Department of Otorhinolaryngology
Section of Experimental Oncology and Nanomedicine

arXiv:1704.04206v1 [cs.ET] 13 Apr 2017

ABSTRACT

In this paper, we propose to use magnetic nanoparticles as information carriers for molecular communication. This enables the use of an external magnetic field to guide information-carrying particles towards the receiver. We show that the particle movement can be mathematically modeled as diffusion with drift. Thereby, we reveal that the key parameters determining the magnetic force are particle size and *magnetic field gradient*. As an example, we consider magnetic nanoparticle based communication in a blood vessel. For this bounded environment, we derive an analytical expression for the channel impulse response subject to fluid flow and magnetic drift. Numerical results, obtained by particle-based simulation, validate the accuracy of the derived analytical expressions. Furthermore, adopting the symbol error rate as performance metric, we show that using magnetic nanoparticles facilitates reliable communication, even in the presence of fluid flow.

1 INTRODUCTION

Molecular communication (MC) is one of the mechanisms that biological cells use to communicate with each other [1, Ch. 16]. In natural MC systems information is conveyed by specific patterns of molecule releases, e.g., by releasing different numbers or types of molecules. Thereby, in typical diffusive MC environments, the *information molecules* propagate by *Brownian motion* where the movement of particles is due to thermally induced collisions with molecules of the embedding liquid.

A recent trend in biotechnology is to create artificial and genetically modified cells [1, Ch. 10]. These synthetic *nanomachines*, e.g., drug bearing cells, could cooperate and fight a local infection site by adjusting the release of the pharmaceutical in a coordinated and controlled manner [10, Ch. 8]. For this smart collaboration of nanomachines, communication is essential. Thereby, a message might trigger a certain chemical process which in turn may cause a desired action of a receiving nanomachine. In this context, MC has recently attracted considerable attention as a biocompatible approach for synthetic communication at the cellular level.

For MC, usually naturally occurring information molecules such as proteins are considered as information carriers [11, Ch. 2]. However, apart from problems in realizing synthetic biological MC systems at nanoscale [5], there are also severe limitations by design. In particular, the movement of the information carriers is random and cannot be stirred towards the receiver, i.e., many of the released molecules do not arrive at the receiver. Moreover, molecules suspended in a fluid are very sensitive to fluid flow which easily dominates the diffusive movement and in many cases cannot be controlled externally, e.g., in blood vessels. In this paper, we will show that these problems can be overcome by using magnetic nanoparticles (MNPs) as information carriers and by guiding them via an external magnetic field.

For targeted drug delivery and many other biotechnological applications, MNPs are widely used already [14]. These particles usually consist of a polymer matrix with embedded iron oxides which we will simply refer to as *magnetic core*, and a nonmagnetic coating. The coating ensures biocompatibility and stability, i.e., it prevents agglomeration of the nanoparticles. Moreover, the particle surface can be *functionalized* with binding sites that are selective to specific molecules [18]. In this way, MNPs can be chemically recognized by cells. Also, by exploiting their magnetic properties, MNPs can be detected by external devices [14]. However most importantly, MNPs can be externally guided by applying a magnetic field. Thereby, the magnetic force crucially depends on the magnetic field gradient rather than the magnitude of the magnetic field. Thus, larger forces can be realized by optimizing the design of the magnet to achieve large magnetic field gradients, see e.g. [16] where the arrangement of spatial arrays of permanent magnets is optimized for this purpose.

Despite their widespread use in contemporary biotechnology, to the best of our knowledge, for synthetic MC, MNPs have only been considered in [8, 11]. In particular, the authors of [11] proposed that MNPs attached to DNA can initiate gene expression if subjected to an external magnetic field. On the other hand, a wearable device detecting changes of inductance when MNPs pass through a coil was devised in [8]. However, to the best of the author's knowledge, using MNPs as information carriers and guiding them by an external magnetic field has not been investigated yet.

Motivated by the general availability and applicability of MNPs in biotechnology, in this paper, we make the following contributions:

(1) We propose the use of MNPs as information carriers and characterize their physical properties. Thereby, we model the particle movement in an external magnetic field as diffusion with drift similar to fluid flow. In contrast to fluid flow, a magnetic field can be directed in a desired direction and even towards solid boundaries. Moreover, we show that the magnetic force critically depends on the particle size.
(2) To illustrate the utility of using MNPs for MC in a realistic environment, we consider a two-dimensional model of a blood vessel and analyze the time-variant spatial particle distribution subject to the combined effect of fluid flow and magnetic drift. As particles usually differ in size, we also

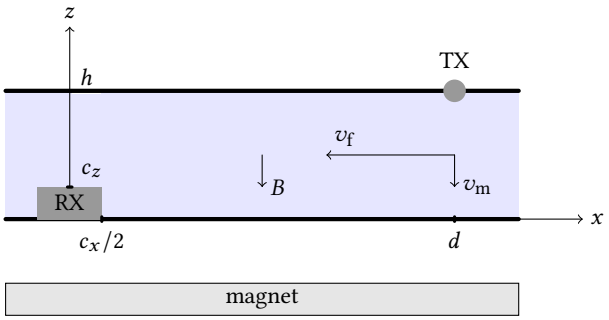

Figure 1: System model geometry.

take into account the typical log-normal distribution of the particle radius [7] in our mathematical expressions.

(3) For the considered model, we calculate the symbol error rate (SER) to evaluate the system performance. Thereby, the system is affected by fluid flow which may prevent information-carrying particles from reaching the receiver (RX). We show that applying a magnetic force can drastically reduce the SER.

The remainder of this paper is organized as follows. In Section 2, we introduce the system model and the magnetic properties of MNPs. Based on this model, we derive the exact particle distribution and channel impulse response in Section 3. Simulation results are provided in Section 4. Finally, Section 5 concludes the paper.

2 SYSTEM MODEL

The use of MNPs can be beneficial for many environments and applications especially when fluid flow hinders MC. As one example where MNPs can be advantageous, we consider a bounded two-dimensional environment of height h and infinite width in the x-z-plane, which could be used as a simple model of a blood vessel. In particular, particles can only diffuse within $-\infty < x < \infty, 0 \leq z \leq h$ and the boundaries at $z = 0$ and $z = h$ are modeled as reflective, see Fig. 1. For this channel, we assume the transmitter (TX) positioned at $x = d, z = h$ wants to deliver a message to the RX which is located on the opposite side at $x = 0, z = 0$. Thereby, fluid flow with velocity v_f carries the MNPs downstream in negative x-direction but possibly past the RX. To increase the number of particles arriving at the RX, a magnet creating a magnetic field B is placed below the channel dragging particles in negative z-direction towards the RX with velocity v_m.

2.1 Channel Model

To illustrate the benefits of using MNPs, we focus on the following common MC model. The binary information symbols, $b[k]$, are modulated by on-off keying (OOK). Assuming instantaneous particle release, for transmitting $b[k] = 1$ and $b[k] = 0$, the point source TX releases N_{TX} and 0 particles, respectively. The RX is a transparent rectangular patch at $|x| \leq c_x/2,\ 0 \leq z \leq c_z$ at the bottom of the channel with height c_z and width c_x. We assume that the RX is perfectly synchronized with the TX, i.e., the RX knows the symbol interval T and when transmission starts and ends, see [6] for more details. By counting the number of particles within its volume, the RX takes samples at times $kT + t_0$, where t_0 is the time offset after which, for each symbol interval, k, particles can be expected within the receiver volume. For detection, in each symbol interval, the number of counted particles at the RX, $n_{RX}[k]$, is compared to a threshold ξ, i.e., the detected symbols are given by

$$\hat{b}[k] = \begin{cases} 0, & n_{RX}[k] < \xi \\ 1, & n_{RX}[k] \geq \xi. \end{cases} \tag{1}$$

2.2 Magnetic Nanoparticles

We model the MNPs by the radius of the magnetic core and the radius including the coating which are denoted as R_m and R_h, respectively. Because of slight variations in the physical parameters during MNP synthesis, actual particle sizes may differ from the intended size. Thereby, it has been found that the log-normal distribution usually provides a good fit to the experimentally observed particle sizes [7]. Motivated by this, for the particle radius, R_m, we assume a log-normal distribution with mean m_R and standard deviation s_R. Thereby, for simplicity, we assume that $R_h = R_m + R_c$, where R_c is the constant thickness of the coating. In the remainder of this paper, we will refer to m_R as the *nominal* particle size, i.e., the target magnetic core size in the production of the MNPs.

We model the externally applied magnetic field by the magnitude of the magnetic flux density B. Thereby, B is assumed to increase towards the magnet, i.e., the gradient of B is in the negative z-direction, cf. Fig. 1. MNPs tend to magnetically align with the applied magnetic field B. However, immersed in a fluid of temperature T_f, the alignment is not perfect. In particular, considering the thermal energy per particle $k_B T_f$, where $k_B \approx 1.381 \times 10^{-23}\ \mathrm{m^2 kg/s^2/K}$ is the Boltzmann constant [12], the average magnetization in the direction of the magnetic field is given by [4, Ch. 4.3.2]

$$M(B) = M_s L\left(\frac{V_m M_s B}{k_B T_f}\right), \tag{2}$$

where the *Langevin function* $L(s)$ is defined as $L(s) = \coth(s) - 1/s$ and $\coth(s)$ is the hyperbolic cotangent. Moreover, V_m is the volume of the magnetic core and M_s denotes the saturation magnetization which applies if the MNP is fully aligned with the applied magnetic field, i.e., $M(B \to \infty) = M_s$. In the remainder of this paper, for simplicity, we will assume $M(B) \approx M_s$. The validity of this assumption is investigated in Section 4, Fig. 2. Eq. (2) implies $M(B = 0) = 0$, which is in contrast to larger ferromagnetic materials for which M does not only depend on the current value of B but also on previous values of B which is an effect known as *hysteresis*.

Given the volume of the magnetic core V_m and its average magnetization in (2), the force on an MNP in a magnetic field B in negative z-direction (cf. Fig. 1) is given by [2]

$$F_m(z) = V_m M_s \frac{\partial}{\partial z} B(z), \tag{3}$$

which is proportional to the magnetic field gradient. In this paper, we assume that the magnetic field within the channel can be accurately described by an affine function of z, i.e., we consider the linearization of $B(z)$. In this case, the magnetic force on the MNPs is constant. Thereby, the force points towards the magnet because this is the direction of increasing magnetic field strength.

The movement of the MNPs is subject to diffusion, which can be characterized by the diffusion coefficient D, and a magnetic drift

with velocity v_m, which is due to the magnetic force F_m. It is known that applying a force F_m on an MNP immersed in a liquid of viscosity η quickly accelerates it to the terminal velocity $v_\mathrm{m} = F_\mathrm{m}/\zeta$ [12, Eq. (4.12)], where ζ is the friction coefficient which by Stokes' law is given by $\zeta = 6\pi\eta R_\mathrm{h}$. In summary, we obtain

$$v_\mathrm{m} = \frac{2M_\mathrm{s}}{9\eta}\frac{R_\mathrm{m}^3}{R_\mathrm{m}+R_\mathrm{c}}\frac{\partial}{\partial z}B(z), \tag{4}$$

which is proportional to the magnetic field gradient and strongly depends on the particle size.

By thermodynamical reasoning [12, Ch. 4], ζ is linked to the diffusion coefficient D by the Einstein relation $k_\mathrm{B}T_\mathrm{f} = D\zeta$. Hence, given the viscosity η and the temperature of the fluid T_f, D can be determined as

$$D = \frac{k_\mathrm{B}T_\mathrm{f}}{6\pi\eta(R_\mathrm{m}+R_\mathrm{c})}, \tag{5}$$

which also depends on the particle size but to a lesser degree than v_m. In contrast, the fluid flow velocity v_f is not affected by changes of R_m.

3 PERFORMANCE ANALYSIS

In this section, we derive an analytical expression for the time-variant spatial MNP distribution by solving the diffusion equation with drift for the system in Fig. 1. Then, equipped with the solution to the diffusion equation, we calculate the probability of observing a particle within the RX volume as well as the expected number of particles which is a function of time that we will refer to as *impulse response*. Finally, given the impulse response, we determine the average received signal and the SER.

3.1 Impulse Response

In the environment depicted in Fig. 1, the particle movement in the x- and z-direction is uncoupled and hence the time-varying probability density function (PDF) for the MNP position can be written as $p(x,z;t) = p_x(x;t)p_z(z;t)$. In this equation, the horizontal distribution $p_x(x;t)$ corresponds to an unbounded environment with constant drift v_f. Hence, this distribution is readily obtained as [17, Eq. (4.39)]

$$p_x(x;t) = \frac{1}{\sqrt{4D\pi t}}\,\mathrm{e}^{-(x+d-v_\mathrm{f}t)^2/(4Dt)}, \tag{6}$$

where the mean particle x-coordinate arrives at the RX at time $t_1 = d/v_\mathrm{f}$. Determining the vertical distribution $p_z(z;t)$ is more challenging because of the combination of a bounded environment and particle drift. Therefore, we consider the underlying partial differential equation (PDE) which is the diffusion equation with drift. Thereby, the reflective boundary conditions are specified by [17, Eq. (4.24)] $D\frac{\partial}{\partial z}p_z(z;t) + v_\mathrm{m}p_z(z;t) = 0$ for $z = 0, h$, and $t > 0$. Moreover, by assumption of a point source TX, the initial position $z_0 = h$ is known a priori. Hence, $p_z(z;t)$ for $t > 0$ is obtained by solving the following PDE with boundary and initial conditions

$$\begin{aligned}
\frac{\partial}{\partial t}p_z(z;t) &= v_\mathrm{m}\frac{\partial}{\partial z}p_z(z;t) + D\frac{\partial^2}{\partial z^2}p_z(z;t), && 0 < z < h\\
\frac{\partial}{\partial z}p_z(z;t) &= -\frac{v_\mathrm{m}}{D}p_z(z;t), && z = 0, h\\
p_z(z;t) &= \delta(z-z_0), && t = 0.
\end{aligned} \tag{7}$$

Solutions to the one-dimensional diffusion equation without drift are well known for various boundary conditions [3]. Motivated by this, using a variable substitution, we obtain an equivalent problem formulation in terms of an auxiliary function $q(z;t)$ without drift term but with $q(z;t\to\infty) = 0$ and modified boundary conditions [15]. To this end, we define $q(z;t)$ by

$$p_z(z;t) = q(z;t)\,\mathrm{e}^{-v_\mathrm{m}(z-z_0)/(2D)-v_\mathrm{m}^2t/(4D)} + p_z^\mathrm{eq}(z), \tag{8}$$

where $p_z^\mathrm{eq}(z) = p_z(z;t\to\infty)$ is the steady state or *equilibrium* solution of (7). Substituting (8) in (7), for $t > 0$ we obtain the following PDE in $q(z;t)$

$$\begin{aligned}
\frac{\partial}{\partial t}q(z;t) &= D\frac{\partial^2}{\partial z^2}q(z;t), && 0 < z < h\\
\frac{\partial}{\partial z}q(z;t) &= -\frac{v_\mathrm{m}}{2D}q(z;t), && z = 0, h\\
q(z;t) &= \delta(z-z_0) - p_z^\mathrm{eq}(z)\,\mathrm{e}^{v_\mathrm{m}(z-z_0)/(2D)}, && t = 0.
\end{aligned} \tag{9}$$

Clearly, to obtain $p_z(z;t)$ in (8), we require $p_z^\mathrm{eq}(z)$. Therefore, in the following, we first give the steady state solution and then use it to solve the original problem.

3.1.1 Steady State. The steady state solution of $p_z(z;t)$ also needs to satisfy (7) but is characterized by $\frac{\partial}{\partial t}p_z(z;t) = 0$, i.e., the following ordinary differential equation (ODE)

$$-\frac{v_\mathrm{m}}{D}p_z^\mathrm{eq}(z) = \frac{\partial}{\partial z}p_z^\mathrm{eq}(z), \quad z\in[0,h] \tag{10}$$

has to be solved. As $p_z^\mathrm{eq}(z)$ is a PDF and no particles are lost, the reflective boundary conditions are met if the steady state PDF satisfies $\int_0^h p_z^\mathrm{eq}(z)\,\mathrm{d}z = 1$.

As can be verified by substitution, (10) is solved by

$$p_z^\mathrm{eq}(z) = s^{-1}\,\mathrm{e}^{-v_\mathrm{m}z/D}, \tag{11}$$

where $s = D\left(1-\mathrm{e}^{-v_\mathrm{m}h/D}\right)/v_\mathrm{m}$.

3.1.2 Transient Solution. As shown in [15], the auxiliary function $q(z;t)$ can be expressed as a series with coefficients a_n

$$q(z;t) = \sum_{n=1}^{\infty} Z_n(z)\,\mathrm{e}^{-s_n^2t}\,a_n, \tag{12}$$

where s_n and $Z_n(z)$, $n = 1, 2, \ldots$, need to satisfy

$$\begin{aligned}
\frac{\partial^2}{\partial z^2}Z_n(z) + s_n^2Z_n(z) &= 0, && 0 < z < h\\
\frac{\partial}{\partial z}Z_n(z) + \frac{v_\mathrm{m}}{2D}Z_n(z) &= 0, && z = 0, h\\
\int_0^h Z_{n_1}(z)Z_{n_2}(z)\,\mathrm{d}z &= \delta_{n_1,n_2},
\end{aligned} \tag{13}$$

where δ_{n_1,n_2} is equal to 0 and 1 for $n_1 \neq n_2$ and $n_1 = n_2$, respectively. Hence, the functions $Z_n(z)$ are normalized orthogonal, and satisfy the boundary conditions of (9). We note that a problem similar to (9) is solved in [3, Ch. 14.3]. In fact, we find that the solution to (13) is given by [3, Ch. 14.3, Eq. (5)]

$$Z_n(z) = \sqrt{\frac{2}{h(s_n^2 + v_\mathrm{m}^2/(4D^2))}}\left(s_n\cos(s_nz) - \frac{v_\mathrm{m}}{2D}\sin(s_nz)\right), \tag{14}$$

where $s_n = n\pi/h$ as can be verified by substitution. Proceeding in solving (9), the coefficients a_n can be calculated by [15, Eq. (17c)]

$$a_n = Z_n(z_0) - \int_0^h Z_n(z) p_z^{\mathrm{eq}}(z)\, \mathrm{e}^{v_{\mathrm{m}}(z-z_0)/(2D)}\, \mathrm{d}z, \tag{15}$$

which simplifies to $a_n = Z_n(z_0)$ because the second integral vanishes.

We are now ready to determine $p_z(z;t)$ by substituting (11) and (12) in (8). In summary, we obtain

$$p_z(z;t) = p_z^{\mathrm{eq}}(z) + \mathrm{e}^{-v_{\mathrm{m}}(z-z_0)/(2D)} \times \sum_{n=1}^{\infty} \mathrm{e}^{-\left(Ds_n^2 + v_{\mathrm{m}}^2/(4D)\right)t} Z_n(z) Z_n(z_0), \tag{16}$$

which simplifies to (11) for $t \to \infty$.

3.1.3 Probability of Particle Observation. Using the PDF $p(x,z;t)$, we can now obtain the probability of observing a particle within the RX volume, $P_{\mathrm{ob}}(t)$, as

$$P_{\mathrm{ob}}(t) = P_{\mathrm{ob},x}(t) P_{\mathrm{ob},z}(t), \tag{17}$$

where $P_{\mathrm{ob},x}(t)$ and $P_{\mathrm{ob},z}(t)$ are the probabilities of observing a particle within the RX x- and z-coordinates $[-c_x/2, c_x/2]$ and $[0, c_z]$, respectively. Integrating (6) from $-c_x/2$ to $c_x/2$ yields

$$P_{\mathrm{ob},x}(t) = \frac{1}{2}\left[\mathrm{erf}\left(\frac{d - v_{\mathrm{f}}t + \frac{1}{2}c_x}{\sqrt{4Dt}}\right) - \mathrm{erf}\left(\frac{d - v_{\mathrm{f}}t - \frac{1}{2}c_x}{\sqrt{4Dt}}\right)\right]. \tag{18}$$

Furthermore, integrating (16) from 0 to c_z yields $P_{\mathrm{ob},z}(t)$ as

$$P_{\mathrm{ob},z}(t) = P_{\mathrm{ob},z}^{\mathrm{eq}} + \mathrm{e}^{-v_{\mathrm{m}}(c_z-z_0)/(2D)} \times \sum_{n=1}^{\infty} \mathrm{e}^{-\left(Ds_n^2 + v_{\mathrm{m}}^2/(4D)\right)t} L_n(z) Z_n(z_0), \tag{19}$$

where $L_n = \int_0^h Z_n(z)\, \mathrm{d}z$ is straightforwardly obtained as

$$L_n = \sqrt{\frac{2}{h(s_n^2 + v_{\mathrm{m}}^2/(4D^2))}} \sin(s_n c_z), \tag{20}$$

and $P_{\mathrm{ob},z}^{\mathrm{eq}}$ is the integral of (11) which is easily found as

$$P_{\mathrm{ob},z}^{\mathrm{eq}} = \frac{1 - \mathrm{e}^{-v_{\mathrm{m}}c_z/D}}{1 - \mathrm{e}^{-v_{\mathrm{m}}h/D}}. \tag{21}$$

We note that $P_{\mathrm{ob},z}(t)$ in (19) is the sum of a transient term approaching zero for $t \to \infty$ and a constant steady state term. Therefore, we can make the following *equilibrium approximation*. If transmitter and receiver are placed far apart, at time t_1 when the particles are expected at the x-coordinates of the receiver, $p_z(z;t)$ will have converged to $p_z^{\mathrm{eq}}(z)$. Consequently, in this case, the particle observation probability reduces to $P_{\mathrm{ob}}(t) = P_{\mathrm{ob},x}(t) P_{\mathrm{ob},z}^{\mathrm{eq}}$, which is a simple scaling of $P_{\mathrm{ob},x}(t)$ in (18). By considering $P_{\mathrm{ob},z}^{\mathrm{eq}}$ in (21), we can also gain qualitative insight on how the particle distribution is affected by changes of the magnetic drift velocity v_{m}. In particular, for $v_{\mathrm{m}} \to 0$ we obtain $P_{\mathrm{ob},z}^{\mathrm{eq}} = c_z/h$ as in this case the particle distribution is uniform across the blood vessel height because of diffusion. On the other hand, for $v_{\mathrm{m}} \to \infty$ we obtain $P_{\mathrm{ob},z}^{\mathrm{eq}} = 1$, i.e., all particles are gathered at the lower boundary in Fig. 1 since the magnetic drift completely dominates diffusion.

Having obtained the particle observation probability at the receiver (17), we can now obtain the expected number of received molecules as a function of time due to the release of N_{TX} particles. Thereby, assuming the number of particles within the channel is small enough such that particle interactions can be ignored, we obtain the *impulse response*

$$\overline{N}_{\mathrm{ob}}(t) = \sum_{i=1}^{N_{\mathrm{TX}}} P_{\mathrm{ob},i}(t), \tag{22}$$

where $P_{\mathrm{ob},i}(t)$ is the probability of observing particle i at time t. Thereby, $P_{\mathrm{ob},i}(t)$, $i = 1, 2, \ldots, N_{\mathrm{TX}}$, are different for $s_R > 0$ where particle sizes differ. In particular, in (18) and (19), v_{m} and D depend on R_{m} via (4) and (5). On the other hand, for $s_R = 0$, we have $P_{\mathrm{ob},i}(t) = P_{\mathrm{ob}}(t)$, $\forall i$, i.e., all particles have the same (nominal) particle size m_R. In this case, $\overline{N}_{\mathrm{ob}}(t) = N_{\mathrm{TX}} P_{\mathrm{ob}}(t)$ which we will refer to as the *nominal impulse response*.

3.2 Symbol Error Rate

Using [13, Eq. (30)], the average number of observed particles $\overline{n}_{\mathrm{RX}}[k]$ in the k-th time slot due to a binary sequence b of transmitted symbols $b[k] \in \{0, 1\}$, $0 \le k < K$ is given by

$$\overline{n}_{\mathrm{RX}}[k] = \sum_{i=0}^{k} b[i] \overline{N}_{\mathrm{ob}}((k-i)T + t_0). \tag{23}$$

Assuming that the only impairments are the random diffusive arrivals of the particles and inter-symbol interference (ISI) by previously released molecules, we define the *average* SER as

$$P_{\mathrm{e}} = \frac{1}{2^K} \sum_{b \in \mathbb{B}(K)} \left[\frac{1}{K} \sum_{k=0}^{K-1} \Pr\left(\hat{b}[k] \neq b[k];\ b[\kappa \le k]\right)\right], \tag{24}$$

where $\mathbb{B}(K)$ is the set of all 2^K possible binary sequences of length K and $\Pr\left(\hat{b}[k] \neq b[k];\ b[\kappa \le k]\right)$ is the probability of detecting $b[k]$ incorrectly given the transmitted sequence $b[\kappa]$ for $0 \le \kappa \le k$.

In general, using the detection in (1), the probability of making an error for the k-th symbol can be written as

$$\Pr(\hat{b}[k] \neq b[k];\ b[\kappa \le k]) = \begin{cases} p_\xi, & b[k] = 1 \\ 1 - p_\xi, & b[k] = 0, \end{cases} \tag{25}$$

where $p_\xi = \Pr(n_{\mathrm{RX}}[k] < \xi;\ b[\kappa \le k])$ is the probability of observing less than ξ MNPs at the k-th sampling time given $b[\kappa]$ for $0 \le \kappa \le k$. Similar to [13], $n_{\mathrm{RX}}[k]$ can be well approximated by a Poisson random variable with mean $\overline{n}_{\mathrm{RX}}[k]$, see [9]. In this case, $p_\xi = \Pr(n_{\mathrm{RX}}[k] \le \xi - 1;\ b[\kappa \le k])$ is the Poisson *cumulative distribution function* with mean $\overline{n}_{\mathrm{RX}}[k]$ evaluated at $\xi - 1$.

If there is no ISI, then for any $\xi \ge 1$, $b[k] = 0$ is always detected correctly because in this case $\overline{n}_{\mathrm{RX}}[k] = 0$. On the other hand, if $b[k] = 1$, then $\overline{n}_{\mathrm{RX}}[k] = \overline{N}_{\mathrm{ob}}(t_0)$ and detection is correct most often for the minimal ξ. Hence, assuming there is no ISI, $\xi = 1$ minimizes P_{e}. In this case, an error occurs only if $b[k] = 1$ and $n_{\mathrm{RX}}[k] = 0$. Hence, (24) simplifies to $P_{\mathrm{e}} = 1/2 \times \Pr(n_{\mathrm{RX}}[k] = 0;\ b[k] = 1)$ assuming $\Pr(b[k] = 1) = 1/2$. For Poisson random variable $n_{\mathrm{RX}}[k]$, the average SER simplifies to

$$P_{\mathrm{e}} = \frac{1}{2}\, \mathrm{e}^{-\overline{N}_{\mathrm{ob}}(t_0)}, \tag{26}$$

Table 1: System parameters using the viscosity of water for η, room temperature for T_f, a saturation magnetization similar to magnetite for M_s, a magnetic field gradient well below realizable values for $\frac{\partial}{\partial z}B$ [2], the diameter of a human capillary for h, and the central blood velocity in capillaries for v_f [1].

Parameter	Value	Parameter	Value
η	$1 \times 10^{-3}\,\mathrm{kg\,m^{-1}\,s^{-1}}$	d	1 mm
T_f	300 K	h	10 µm
R_c	1 nm	c_x	0.1 mm
m_R	50 nm	c_z	1 µm
s_R	10 nm	v_f	$0.5\,\mathrm{mm\,s^{-1}}$
M_s	$5 \times 10^5\,\mathrm{A\,m^{-1}}$	T	2 s
$\frac{\partial}{\partial z}B$	$5\,\mathrm{T\,m^{-1}}$	ξ	1

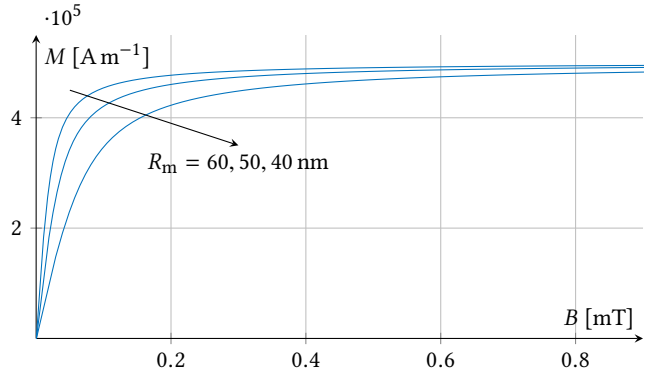

Figure 2: Magnetization curves as given by (2) for magnetic core sizes $R_\mathrm{m} = 40, 50, 60$ nm.

which we will refer to as the *no ISI approximation*.

4 NUMERICAL RESULTS

In this section, unless explicitly stated otherwise, we adopt the physical parameters in Table 1. Thereby, we choose $t_0 = t_1$, where $t_1 = d/v_\mathrm{f}$, i.e., the RX takes a sample when particles are expected due to fluid flow. For simulation of the system described in Section 2, we use a particle-based approach where time advances in discrete time steps Δt and the position of each particle is tracked and updated in each time step, see e.g. [5, Eq. (1)]. Then, for the received signal, for each time step, the number of particles within the receiver volume is counted. Within each simulation step, if a particle crosses a channel boundary, it is reflected back into the channel.

In Fig. 2, we evaluate the particle magnetization (2) as a function of the applied magnetic field B for $R_m = m_R$ and $R_m = m_R \pm s_R$. As $M(B)$ in (2) is point symmetric, we only show $M(B)$ for $B \geq 0$. Here, magnetization is saturated already for $B \approx 1$ mT which is easily exceeded by today's magnets for targeted drug delivery [2]. Hence, assuming $M(B) \approx M_\mathrm{s}$ in Section 2, is justified. Compared to the nominal particle size, slightly larger and smaller MNPs reach saturation quicker and slower because their magnetization direction is less and more affected by thermal energy, respectively.

In Fig. 3, we show the fraction of MNPs within the receiver volume after a point release of N_TX particles at the transmitter at $t = 0$ as a function of time for times around $t_1 = 2$ s. The curves are parameterized by different magnetic field gradients $\frac{\partial}{\partial z}B$ resulting in different drift velocities v_m. For each $\frac{\partial}{\partial z}B$, we also show the nominal impulse response as well as simulated data points. For clarity, the equilibrium approximation is only shown for $\frac{\partial}{\partial z}B = 5\,\mathrm{T\,m^{-1}}$. Fig. 3 shows that increasing the magnetic field gradient significantly increases the number of observed MNPs. There is a time window of approximately 0.2 s centered around $t_1 = 2$ s within which a nonzero number of MNPs can be observed independent of the magnetic field gradient. Hence, for a symbol interval size of $T = 2$ s, ISI does not play a significant role for the given parameters due to the flow-dominated transport of particles. Due to the log-normal particle size distribution there is some deviation from the nominal impulse response as v_m depends on the particle size. In particular, when $\frac{\partial}{\partial z}B$ is relatively small (e.g. $\frac{\partial}{\partial z}B = 5\,\mathrm{T\,m^{-1}}$) and large (e.g. $\frac{\partial}{\partial z}B = 20\,\mathrm{T\,m^{-1}}$), more and fewer MNPs are observed at the RX than expected based on the nominal impulse response, respectively. This can be explained as follows. The nominal impulse response is obtained based on the assumption that the radius of all MNPs is equal to the mean radius m_R. The magnetic force experienced by a particle increases with its size. Hence, for small $\frac{\partial}{\partial z}B$, the magnetic force experienced by MNPs having radius m_R is relatively weak and having MNPs with a larger radius, and thus, experiencing a larger magnetic force, increases the number of observed MNPs. On the other hand, for large $\frac{\partial}{\partial z}B$, the magnetic force experienced by MNPs having radius m_R is relatively strong and almost all MNPs with this radius arrive at the RX. Thus, having even larger MNPs cannot further increase the number of observed MNPs. However, having smaller MNPs, which experience a weaker magnetic force, decreases the number of observed MNPs. Regarding the equilibrium approximation for $\frac{\partial}{\partial z}B = 5\,\mathrm{T\,m^{-1}}$, we see that it overestimates the number of observed particles as within the time frame where MNPs can be observed, the steady state has not yet been reached. Overall, Fig. 3 confirms that magnetically targeting the RX proves effective in increasing the number of observed MNPs. Thereby, for the considered system model, larger magnetic field gradients are preferable.

In Fig. 4, we evaluate the symbol error rate when the magnet is turned on and off, respectively, as a function of the number of MNPs used per transmit pulse. In particular, for each N_TX, we show the SER according to (24) for $\xi = 1$ as well as simulation results for SER $\geq 5 \times 10^{-5}$ where the particle sizes have been chosen independently for each transmit pulse of N_TX particles. As for $T = 2$ s, no ISI is expected for the chosen system parameters, cf. Fig. 3, the no ISI approximation in (26) matches (24) which for clarity is not shown. We can also observe that the system is very sensitive to changes in the fluid flow which can not be controlled externally. However, overall, we note that turning the magnet on reduces the SER significantly.

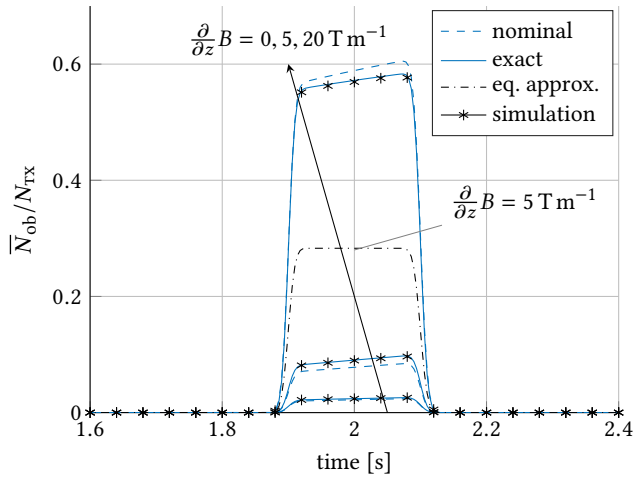

Figure 3: Impulse response $\overline{N}_{\mathrm{ob}}(t)$ in (22) for different magnetic field gradients where $N_{\mathrm{TX}} = 1000$. Simulation results with $\Delta t = 2\,\mathrm{ms}$ have been averaged over 10^4 realizations (for clarity, not all points are shown).

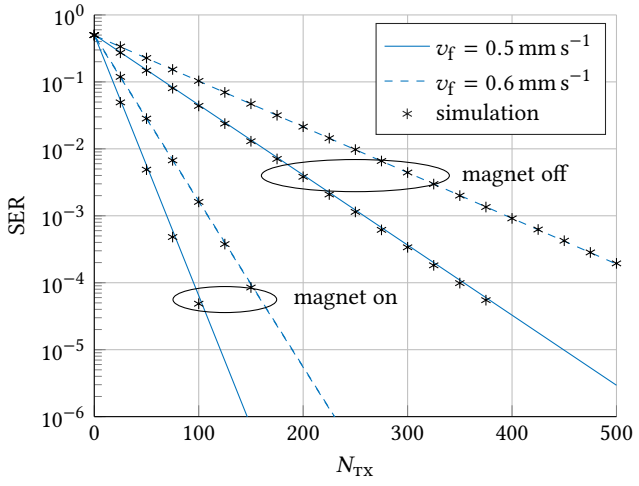

Figure 4: Symbol error rate as a function of the available number of MNPs per symbol. P_{e} in (24) with $K = 10$ is shown for two different fluid flow velocities and with the magnet turned on and off. Simulation results with $\Delta t = 20\,\mathrm{ms}$ have been averaged over 10^6 realizations.

5 CONCLUSION

In this paper, we proposed the use of MNPs as information-carriers for MC systems. In particular, we showed how the movement of MNPs can be modeled as diffusion with drift. To this end, we reviewed the magnetic drift velocity resulting from a magnetic force caused by a magnetic field gradient. Thereby, we highlighted the dependence of the drift velocity and the diffusion coefficient on the particle size. Subsequently, we introduced a technique to solve the diffusion equation with drift in a bounded environment and applied this technique to derive the impulse response in a blood vessel subject to fluid flow, diffusion, and magnetic drift. Moreover, we demonstrated how the particle size distribution can be incorporated in the impulse response. By numerical evaluation, we illustrated how a log-normal particle size distribution affects the impulse response for different magnetic field gradients. Finally, by evaluating the SER, we have shown how sensitive the system is to variations in the fluid flow velocity and how applying an external magnetic field can ensure reliable communication.

ACKNOWLEDGMENTS

This work was supported in part by the Friedrich-Alexander Universität Erlangen-Nürnberg (FAU) under the Emerging Fields Initiative (EFI).

REFERENCES

[1] B. Alberts, D. Bray, K. Hopkin, A. Johnson, J. Lewis, M. Raff, K. Roberts, and P. Walter. 2013. *Essential Cell Biology* (fourth ed.). Garland Science.
[2] C. Alexiou, D. Diehl, P. Henninger, H. Iro, R. Rockelein, W. Schmidt, and H. Weber. 2006. A High Field Gradient Magnet for Magnetic Drug Targeting. *IEEE Trans. Appl. Supercond.* 16 (June 2006), 1527–1530.
[3] H. S. Carslaw and J. C. Jaeger. 1986. *Conduction of Heat in Solids* (second ed.). Oxford University Press.
[4] J. M. D. Coey. 2010. *Magnetism and Magnetic Materials.* Cambridge University Press.
[5] N. Farsad, H. B. Yilmaz, A. Eckford, C. B. Chae, and W. Guo. 2016. A Comprehensive Survey of Recent Advancements in Molecular Communication. *IEEE Commun. Surv. Tutor.* 18 (3rd Quart. 2016), 1887–1919.
[6] V. Jamali, A. Ahmadzadeh, and R. Schober. 2017. Symbol Synchronization for Diffusive Molecular Communication Systems. *Accept. Present. ICC 2017* (Feb. 2017). arXiv:1610.09141
[7] L. B. Kiss, J. Söderlund, G. A. Niklasson, and C. G. Granqvist. 1999. New Approach to the Origin of Lognormal Size Distributions of Nanoparticles. *Nanotechnology* 10 (1999), 25–28.
[8] S. Kisseleff, R. Schober, and W. H. Gerstacker. 2017. Magnetic Nanoparticle Based Interface for Molecular Communication Systems. *IEEE Commun. Lett.* 21 (Feb. 2017), 258–261.
[9] L. Le Cam. 1960. An Approximation Theorem for the Poisson Binomial Distribution. *Pac. J. Math.* 10 (Nov. 1960), 1181–1197.
[10] T. Nakano, A. W. Eckford, and T. Haraguchi. 2013. *Molecular Communication.* Cambridge University Press.
[11] T. Nakano, S. Kobayashi, T. Suda, Y. Okaie, Y. Hiraoka, and T. Haraguchi. 2014. Externally Controllable Molecular Communication. *IEEE J. Sel. Areas Commun.* 32 (Dec. 2014), 2417–2431.
[12] P. Nelson. 2007. *Biological Physics.* W. H. Freeman.
[13] A. Noel, K. C. Cheung, and R. Schober. 2014. Improving Receiver Performance of Diffusive Molecular Communication With Enzymes. *IEEE Trans. NanoBioscience* 13 (March 2014), 31–43.
[14] Q. A. Pankhurst, N. T. K. Thanh, S. K. Jones, and J. Dobson. 2009. Progress in Applications of Magnetic Nanoparticles in Biomedicine. *J. Phys. Appl. Phys.* 42, Article 224001 (Nov. 2009), 15 pages.
[15] J. S. Pérez Guerrero, L. C. G. Pimentel, T. H. Skaggs, and M. T. van Genuchten. 2009. Analytical Solution of the Advection–diffusion Transport Equation Using a Change-of-Variable and Integral Transform Technique. *Int. J. Heat Mass Transf.* 52 (June 2009), 3297–3304.
[16] A. Sarwar, A. Nemirovski, and B. Shapiro. 2012. Optimal Halbach Permanent Magnet Designs for Maximally Pulling and Pushing Nanoparticles. *J. Magn. Magn. Mater.* 324 (March 2012), 742–754.
[17] K. Schulten and I. Kosztin. 2000. Lectures in Theoretical Biophysics. *Univ. Ill.* (April 2000).
[18] O. Veiseh, J. W. Gunn, and M. Zhang. 2010. Design and Fabrication of Magnetic Nanoparticles for Targeted Drug Delivery and Imaging. *Adv. Drug Deliv. Rev.* 62 (March 2010), 284–304.